



## ANN-MPPT BASED SOLAR PV INTEGRATION INTO GRID BY EMPLOYING A MODIFIED SEPIC CONVERTER AND INVERTER

**Peddapally Sandeep**, PG Scholar, Department of Electrical And Electronics Engineering, Jawaharlal Nehru technological University Hyderabad, TS, India email: [chintusandy825@gmail.com](mailto:chintusandy825@gmail.com)  
**Dr. D. Kiran Kumar**, Assistant Professor, Department of Electrical And Electronics Engineering, Jawaharlal Nehru technological University Hyderabad, TS, India email: [kirannkumar9@gmail.com](mailto:kirannkumar9@gmail.com)

### ABSTRACT

In the present paper, an Maximum Power Point Tracking (MPPT) system using Artificial Neural Networks (ANN) for a photovoltaic (PV) array system that integrated with the grid. The suggested approach incorporates a modified Single Ended Primary Inductor Converter (SEPIC) that enhance extraction efficiency and stability of the power conversion process. The Artificial Neural Network algorithm is utilized to achieve and maintain the maximum power point (MPP) quickly under varying environmental factors such variations in temperature and solar irradiation, achieving an efficiency above 99.5%. The simulation results shows enhanced energy harvesting capacity which increased energy production per installed capacity unit, which lowers the Levelized Cost of Energy (LCOE). Additionally, reduced hardware requirements make the system extremely cost-effective. The power extraction is optimized by the application of a modified SEPIC converter whereas the inverter controlled by dq voltage ensures synchronization and power quality for grid integration. Total Harmonic Distortion (THD) that is equivalent to or less than 0.66% in the inverter current and power obtained from a solar PV was under 1% variation. The results reveal remarkable enhancements for both energy harvesting and system stability, which makes the presented system is suitable to be employed in future advanced solar PV installations.

### Keywords:

Maximum Power Point Tracking, Artificial Neural Network, Single Ended Primary Inductor Converter, Levelized Cost of Energy.

### I. INTRODUCTION

ANN-based MPPT methods offer high efficiency and improved energy harvesting, resulting in more energy generated per unit of installed capacity, which helps reduce the Levelized Cost of Energy (LCOE). Additionally, these methods can minimize hardware requirements by estimating the Maximum Power Point (MPP) with fewer input parameters, reducing the need for extra sensors and simplifying the system, which ultimately decreases overall hardware and maintenance costs of system. Therefore the system become cost-effective and more economical. Also in last decade, an extensive and accelerating burn of fossil resources has created a dramatic environmental impact [1]. This has led to the interest of researcher for renewable energy sources (RES). The success on the grid-connected photovoltaic systems have become known all over slipped battery charge. which is far expensive and complicated facility. The development of photovoltaic energy conversion has been primarily focused on 2-stage or multi-stage and single-stage system [2].

For instance, current-voltage (I-V) and power-voltage (P-V) characteristics that could impact the performance of photovoltaic systems. The Maximum power point Tracking (MPPT) technique is used to maximize power output. perturb and observe (P&O) [3] and incremental conductance (Inc) [4] are popular MPPT technique in use.

Its cost-effectiveness and simplicity have made algorithms like Fuzzy logic MPPT approaches and artificial neural networks (ANN) are very efficient in terms of performance and computation [5]. Optimized Adaptive Neuro-Fuzzy Interpretation System for Bald Eagle Search A MPPT using performance module was found to have the efficient tracking rate of approximately achieved (98.92%) with faster execution time of 0.24 seconds [6]. Metaheuristically optimized ANN MPPT controller,

implemented using the Horse Herd Optimization algorithm on account of its quickly altering solar irradiance, provides enhanced maximal power tracking performance as well as an improved efficiency and computational time[7].

PV voltage is increased via series and parallel arrangements, but efficiency and system size are sacrificed[8]. Switching capacitors and non-isolated converters have been proposed as high voltage gain methods[9], while modified SEPIC DC-DC converters provide effective low voltage enhancement for DC microgrids, powered cars, and DC homes[10]. The use of grid-tied solar energy systems has increased as they do not require battery storage and the related expenses. Therefore, System become cost-effective. PV conversion systems can be single, two, or multi-stage; multilevel inverters are recommended for high-power applications because they can provide a more pure sinusoidal output and have lower total harmonic distortion (THD)[11]. An inverter synchronizes the DC to AC with the grid while a DC-DC converter modifies the solar power input in a typical two-stage setup[12]. This enables mitigation of the adverse effects of harmonics, promotion in load current balance and unity-power factor etc by providing techniques to improve power quality features like smoothing and energy decoupling without storage[13]. Phase-locked loops (PLLs) synchronize the inverter voltage in order to have a unity power factor with the grid voltage and assure precise phase angle calculation[14]. Grid-integrated signal THD must be less than 5%, according to IEEE standard 519 [15]. This setup allows solar panel power to be increased as needed and injected into the grid. Three-phase reference voltages  $U_a, U_b$  and  $U_c$  generate six PWM pulses used to control a three-phase multilevel inverter [16]. In present suggested system we are going to develop a Solar PV array integrated to grid with Modified SEPIC Converter and develop an ANN block with Bayesian Regularization Algorithm for MPPT.

The performance of the suggested system was determined by the MATLAB/Simulink model under steady state and switching experimental condition to test if both the integrated systems can be feasible or not. The arrangement of the paper is as follows: Chapter one contains intro of the system suggested. The second chapter explains how the system is configured. The control approaches for the system's converter and inverter is described in Section three. The outcomes of the simulation and comments are presented in Chapter four, and the article is concluded in Chapter five.

## II. CONFIGURATION OF SYSTEM

The whole structure of suggested approach illustrates in figure 1.

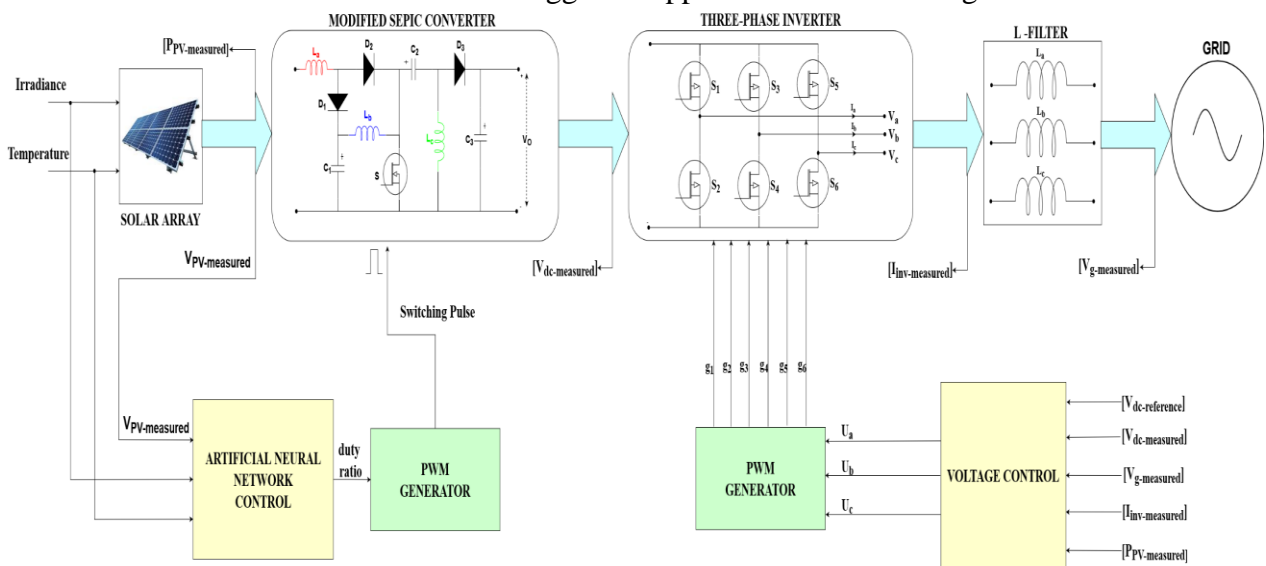


Fig.1.Configuration of the System

### 2.1. DEVELOPING A PV ARRAY MODEL

The basic power transformation unit in a photovoltaic (PV) power generation system is the PV module. The PV module's the outcome is mostly depends on temperature (T) and solar irradiance(G).

Because it is easier to solve the non-linear formulae in a single diode model than in a two-diode one. which requires considerable effort and results in lower computational speed [17,18].

The realistic substitute circuit for a single-diode solar power module model and a PV array model, which comprises a source of current connected parallel along with a diode, has been demonstrated in Figures 2(a) and 2(b). To conduct PV arrays, the PV module is modeled and simulated in Simulink/MATLAB using the parameters given in Table I.

**Table.I. PV Module Specifications**

| S.No | Parameter  | Value            |
|------|--|------------------|
| 1    | Maximum Power, $P_M$                               | 324.974 W        |
| 2    | Voltage during Maximum power point, $V_{MPP}$      | 37.7 V           |
| 3    | Current during maximum power point, $I_{MPP}$      | 8.62 A           |
| 4    | Voltage in an open circuit, $V_{OC}$               | 45.7 V           |
| 5    | Current in an Short circuit, $I_{SC}$              | 9.18 A           |
| 6    | The coefficient of temperature of $V_{OC}$ , $K_V$ | -0.3358 V/K      |
| 7    | The coefficient of temperature of $I_{SC}$ , $K_I$ | 0.102 A/K        |
| 8    | Diode ideality factor, $a$                         | 0.99216          |
| 9    | Cells per module, $n_s$                            | 72               |
| 10   | Shunt resistance, $R_{sh}$                         | 314.708 $\Omega$ |
| 11   | Series resistance, $R_s$                           | 0.28592 $\Omega$ |
| 12   | Diode saturation current, $I_0$                    | 1.3882e-10 A     |
| 13   | Light-generated current, $I_L$                     | 9.1909 A         |

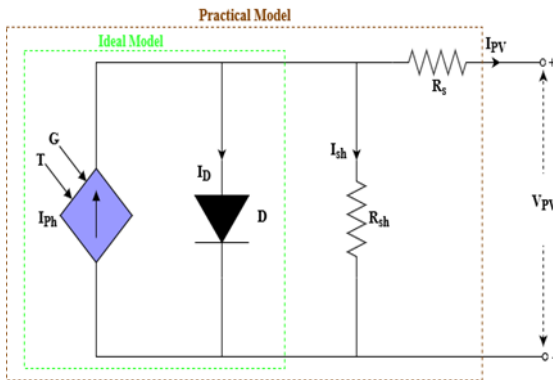
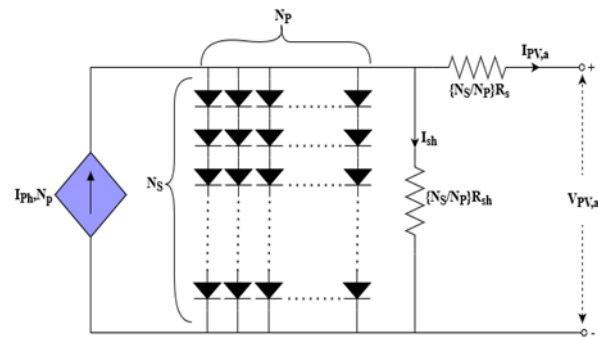


**Fig.2(a) PV module equivalent circuit.**



**2(b).PV Array equivalent circuit.**

Equation (1) provides the link between a PV module's voltage and current mathematically.

$$I_{PV} = I_{ph} - I_r \left[ \exp \left( \frac{q(V_{PV} + R_s I_{PV})}{n_s k T a} \right) - 1 \right] - \frac{V_{PV} + R_s I_{PV}}{R_{sh}} \quad (1)$$

Here,  $I_{PV}$  stands for the photocurrent generated in module (A) as a outcome of solar irradiation and  $V_{PV}$  is the voltage of the PV module (V),  $V_T$  is the thermal voltage of PV module (V),  $I_r$  is the reverse saturation current of the diode (A), T is PV module's operating temperature, k is Boltzmann constant, q is an electron charge,  $R_s$  and  $R_{sh}$  are corresponding to the shunt and series resistances( $\Omega$ ),and a is ideality factor of the diode.

Equation (2) provides the link between a PV array voltage and current mathematically [19].

$$I_{PV,a} = I_{ph} N_p - I_r N_p \left[ \exp \left( \frac{q(V_{PV,a} + R_s \left( \frac{N_s}{N_p} \right) I_{PV,a})}{n_s k T a} \right) - 1 \right] - \frac{V_{PV,a} + R_s \left( \frac{N_s}{N_p} \right) I_{PV,a}}{R_{sh} \left( \frac{N_s}{N_p} \right)} \quad (2)$$

In this context,  $N_s$  specifies the quantity of PV modules are interconnected in series, and  $N_p$  specifies the quantity of PV modules interconnected in parallel,  $I_{PV,a}$  and  $V_{PV,a}$  refer to the output voltage and current of the PV array, correspondingly. The ideal I-V and P-V curves of a PV module are depicted in Figure 2(c).

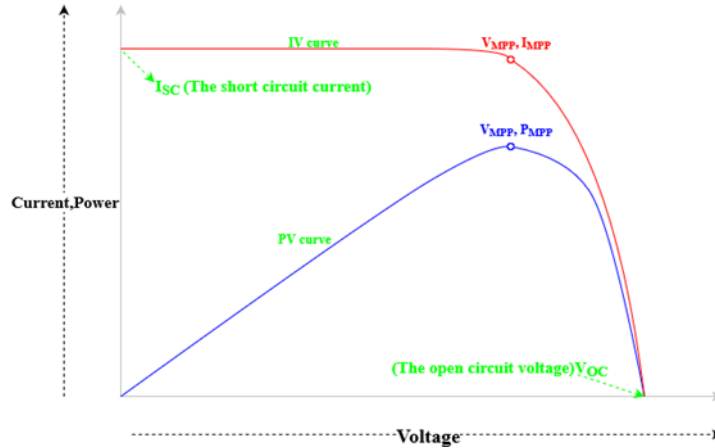


Fig.2(c). I-V and P-V curve of PV Module.

## 2.2. MODIFIED SEPIC CONVERTER

In the present paper, we represent a novel topology for only one switch integrated high gain SEPIC converter which is suitable to deal with the high voltage levels. This has one input and output port made by modifying the traditional SEPIC converter illustrated by Fig.3(a). The MSC power circuit, illustrated by fig.3(b), comprises three inductors ( $L_a$ ,  $L_b$ , and  $L_c$ ), three capacitors ( $C_1$ ,  $C_2$  and  $C_3$ ), and three diodes ( $D_1$ ,  $D_2$  and  $D_3$ ), all managed by an identical switch (S) with a frequency of switching ( $f_s$ ). Together with two diodes, inductor  $L_b$  and capacitor  $C_1$  function as voltage amplification components inside the MSC. The use of only one switch, which streamlines the control circuitry, continuous input current, high voltage gain, and best possible input source utilization are the primary benefits of the proposed MSC.

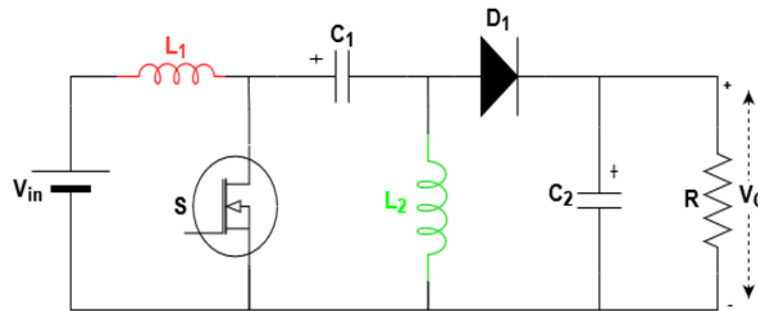


Fig.3(a) Sepic Converter

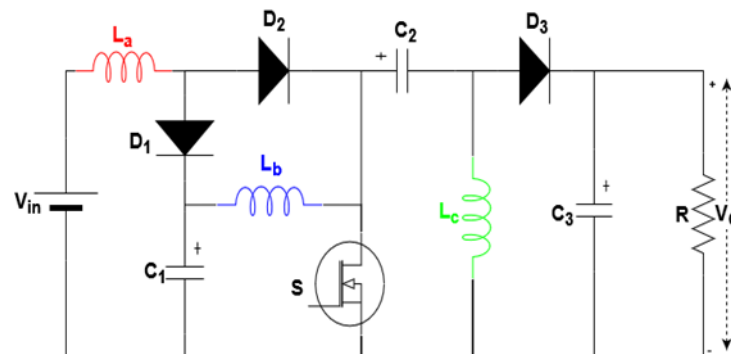


Fig.3(b) Modified Sepic Converter

It has two operating modes  
UGC CARE Group-1

**In mode-1(S-ON):-**The present current flow pathways for the three inductors are described as follows: Inductor  $L_a$  channels current from the input power supply ( $V_{in} - D_2 - S - V_{in}$ ), Inductor  $L_b$  draws current from capacitor  $C_1$  ( $V_{C_1} - V_{L_b} - S - V_{C_1}$ ), and Inductor  $L_c$  draws current from capacitor  $C_2$  ( $V_{C_2} - S - V_{L_c} - V_{C_2}$ )[1]. Concurrently, Diode  $D_3$  is reverse biased by capacitor  $C_3$ , which supplies energy to the electrical load.

**In mode-2(S-OFF):-** The current pathways for all inductors are as follows: Inductor  $L_a$  works with the input voltage  $V_{in}$  to charge capacitor  $C_1$  ( $V_{in} - V_{L_a} - D_1 - C_1 - V_{in}$ ). Capacitor  $C_2$  is energized by inductor  $L_b$  and capacitor  $C_1$  in the following manner: ( $V_{C_1} - V_{L_b} - V_{C_2} - D_3 - V_o - V_{C_1}$ )[1]. Inductor  $L_c$  simultaneously discharges down the load in the following manner: ( $V_{L_c} - D_3 - V_o$ ).

### 2.2.1 DESIGN OF INDUCTORS

$$L_a = \frac{D \cdot V_{in}}{f_{sw} \cdot \Delta I_{L_a}} \tag{3}$$

$$L_b = \frac{D \cdot V_{C_1}}{f_{sw} \cdot \Delta I_{L_b}} = \frac{D \cdot V_{in}}{f_{sw} \cdot (1-D) \cdot \Delta I_{L_b}} \tag{4}$$

$$L_c = \frac{D \cdot V_{C_2}}{f_{sw} \cdot \Delta I_{L_c}} = \frac{D \cdot V_{in}}{f_{sw} \cdot (1-D) \cdot \Delta I_{L_c}} \tag{5}$$

### 2.2.2 DESIGN OF CAPACITORS

$$C_1 = \frac{D \cdot V_{C_1}}{R \cdot \Delta V_{C_1} \cdot f_{sw}} = \frac{D \cdot V_{in}}{R \cdot C_1 \cdot f_{sw} \cdot (1-D)} \tag{6}$$

$$C_2 = \frac{D \cdot V_o}{R \cdot \Delta V_{C_2} \cdot f_{sw}} \tag{7}$$

$$C_3 = \frac{D \cdot V_{C_3}}{R \cdot \Delta V_{C_3} \cdot f_{sw}} \tag{8}$$

Where  $L_a = L_b = L_c$  = Inductors,  $C_1 = C_2 = C_3$  =Capacitors,  $\Delta I_{L_a} = \Delta I_{L_b} = \Delta I_{L_c}$  =Current ripples,  $V_o$ =output voltage,  $V_{in}$  =input voltage,  $D$  =duty ratio,  $\Delta V_{C_1} = \Delta V_{C_2} = \Delta V_{C_3}$  =voltage ripple,  $R$  = Resistance,  $f_{sw}$  =switching frequency,  $V_{C_1} = V_{C_2} = V_{C_3}$  =Voltage across the capacitors.

### 2.3 FILTER DESIGN

Inductive filter used in this project is schematically plotted as on fig.4. Similar to a noise-canceling device for music, the filter subdues irregularities in electrical signals and minimizes high-frequency noise. This process help to secure that clean and stable power is given to the grid, hence protecting equipment and this respect with ruling authority standards[20-23].The inductance for this filter is determined by equation 9.

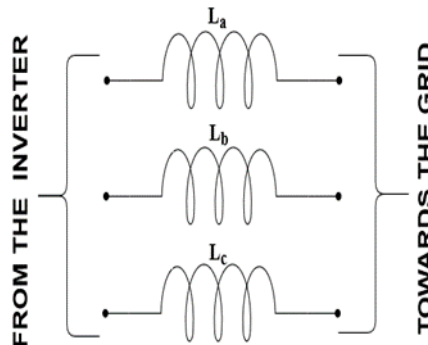


**Fig.4. Inductive Filter**

$$L = L_a = L_b = L_c = \left(\frac{2}{3}\right) \times \left(\frac{m_a V_{dc}(1-m_a)}{2\Delta i_p f_{sw}}\right) \tag{9}$$

Where,  $L_a, L_b, L_c$  are filter inductors  
 $V_{dc}$ : DC Bus voltage  
 $\Delta i_p$ : 0.5% of grid current  
 $f_{sw}$ : Switching frequency  
 $m_a$ : ratio of peak AC to DC Voltage.

### 2.4. VOLTAGE SOURCE INVERTER

A solar system tied to the grid requires an inverter with efficient AC control method which is a necessity for appropriate GRID INTEGRATION. Voltage Source Inverter (three-level inverter based on IGBTs) is employed to export power to the grid. The next chapter delves deep into the control strategy.

## III. CONTROL CONFIGURATION

This chapter covers ANN oriented MPPT control and dq Voltage control of the inverter.

### 3.1 ARTIFICIAL NEURAL NETWORK (ANN) ORIENTED MPPT

The switching pulse for the converter is developed as shown in figure 5. These control circuit helps in order to effectively maximize the solar array's output.

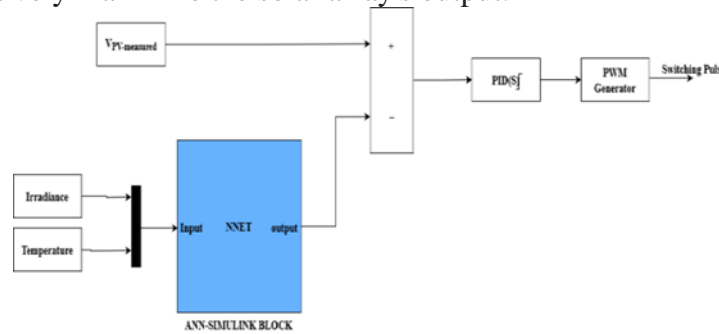


Fig.5. ANN control based MPPT

Here, voltage across the solar array is compared to the generated voltage of the ANN Simulink block. measured across solar array and given to PID controller. PID Controller helps computing the desired actuator output. PWM Generator helps in generating the Switching Pulse.

#### Developing ANN Simulink Block:

An ANN is a type of artificial intelligence approach. Such AI techniques offer several benefits over traditional methods [24]. Traditional methods may not be able to maintain the maximum power point. Figure 6 illustrates the use of ANNs in MPPT.

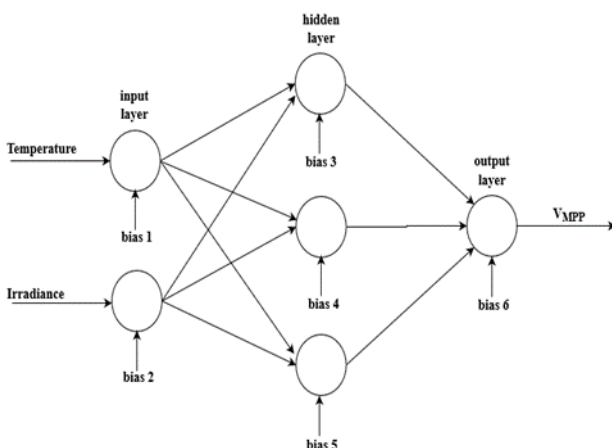


Fig.6. Block diagram of the NN architecture model



Fig.7. Flowchart Of ANN

The process of training of the network involves the use of the Bayesian Regularization (BR) algorithm. The steps for designing an ANN are illustrated in the flowchart above in Fig 7:

- 1.Data gathering
- 2.Choosing the network architecture
- 3.Training the model
- 4.Evaluating the model

### 3.1.1 Data gathering

The Collection of arbitrary temperature and irradiance data from various global locations is generated using a MATLAB program to predict the corresponding irradiance and temperature values (1000 points). By considering the maximum voltage and current data during temperature and irradiation variations, the ANN model is created. The duty ratio for converter switch is produced utilizes the ANN's output (Voltage during Maximum Power Point) based on the provided datasets.

### 3.1.2 Choosing the network architecture

In this research, we examine a feed-forward multilayer network featuring sigmoid hidden neurons and output neurons, as depicted in Figure 8, was utilized for the neural network architecture. This neural network is described to consist of three layers: the hidden layer (active nodes), the output layer (active nodes), and the input layer (passive nodes). The input layer is the primary layer, while the output layer is the final layer. The hidden layer of the neural network architecture used in this model has three hidden neurons, as Figure 6 illustrates.

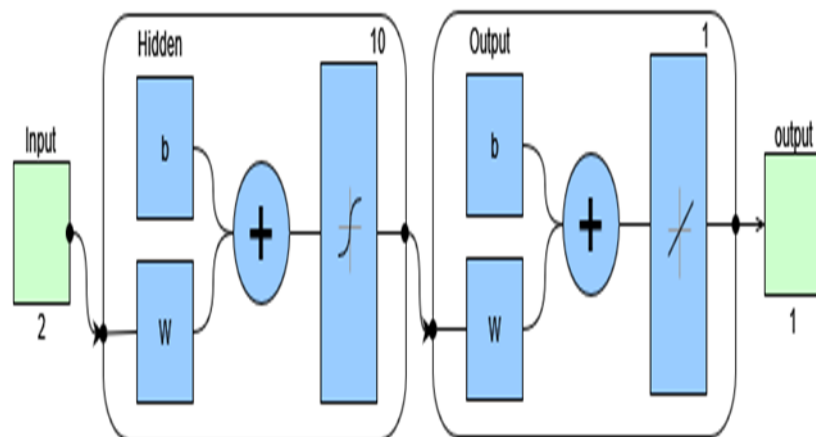


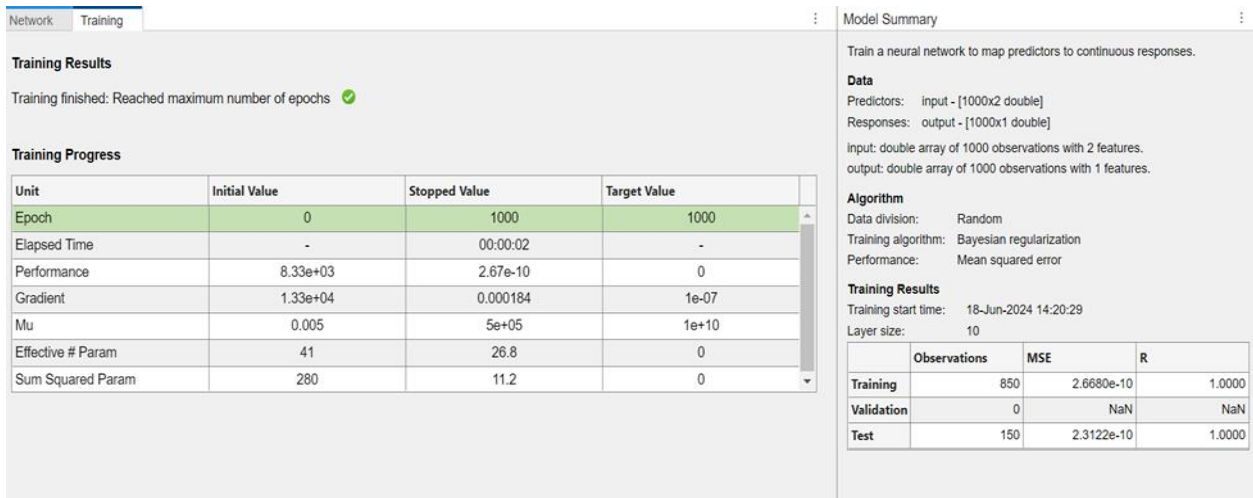
**Fig.8.NN architecture with weight and bias values**

- \* Input : Irradiance and Temperature
- \* Output : Voltage at Maximum Power Point
- \* Sample size:1000
- \* The quantity of hidden neurons:10
- \* The quantity of epochs:1000
- \* Approach : Feed forward methodology
- \* Training data:70%
- \* Validation data:15%
- \* Test data:15%

### 3.1.3 Training the model

The neural network is trained using the "nntool" in MATLAB's m-file. Details of the ANN training are depicted in the fig 9.

**Fig.9 Training details ANN**



For our MPPT model, Bayesian regularized artificial neural networks (BRANNs) were employed due to their superior robustness compared to standard backpropagation networks. A random partition of the data was made, allocating 70% for training, 15% for validation, and 15% for testing. The hidden layer was designed with 10 neurons. Training the ANN datasets involves a number of algorithms [25,26], including LM, BR, and SCG [27]. Regularization is a mathematically sound method that reduces nonlinear regression to a statistically well-posed issue, much to ridge regression. Because it works well even with fewer data points, the training procedure was chosen to use the Bayesian regularization algorithm.

### Bayesian Regularization (BR)

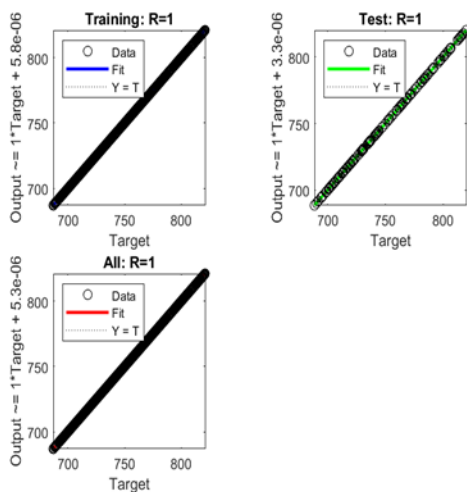


Fig.10. Regression plot of ANN

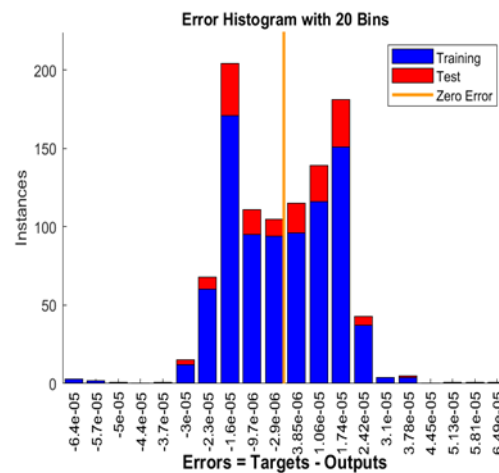
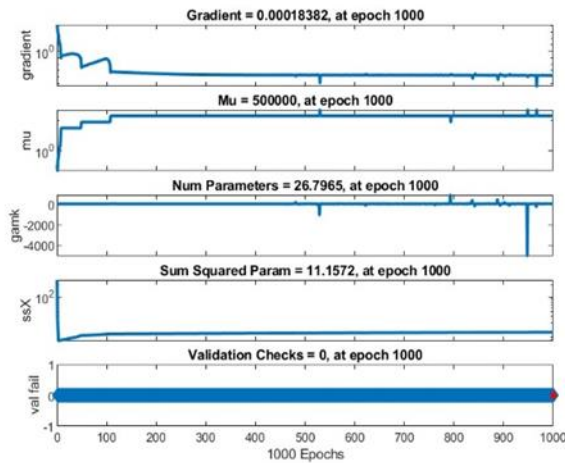


Fig.11. Error Histogram plot of ANN

The neural network's BR method depends on a probabilistic estimations of the network's properties. As a result, as the regression plot in Fig. 10. illustrates. In the regression diagram, a R value of 1 denotes the best possible correlation between the output and the target generated voltage using well calibrated data.

Both the training as well as testing stages of the dataset are shown to have zero error in Figure 11. The overall error fluctuates between 0.000064 (leftmost bin) to 0.0000649 (rightmost bin). In comparison to the LM approach, the error histogram shows a near-zero error of -0.0000029 for 150 samples in the center bin. The gradient and Mu values at 1000 epochs in the training state period demonstrated in Figure 12 are 0.00018382 and 500000, respectively.



**Fig.12 Training Plot of ANN**

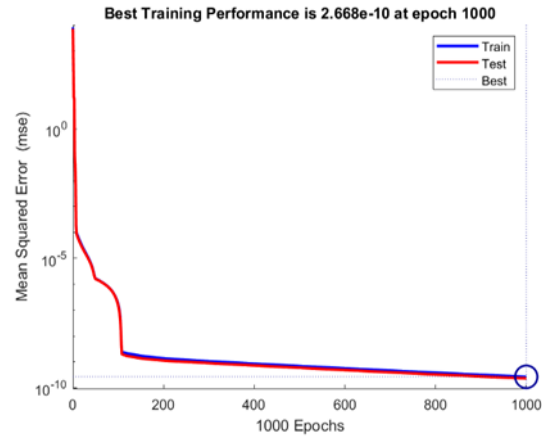


**Fig.13. Performance plot of ANN**

At 1000 epochs, the precise quantity of parameters is 26.7965, and the total of squared parameters is 11.572. As a result, processing training datasets using the BR method takes longer than using the LM approach. The mean squared error at different epochs is shown in Fig. 13, which shows how trained data evolved across 1000 epochs in comparison to the best training outcome. As seen by the best training result of 0.0000000002668 at 1000 epochs, the BR technique is resilient.

### 3.1.4 Evaluating the model

Deploying the model in Simulink and its inner layers are shown in figure 14 and 15 respectively. With the ability to quickly show the Maximum Power Point (MPP) following input parameter settings, this model has made it an extremely useful tool. Furthermore, there is very little latency in generating the result, indicating that the model is quick and effective.

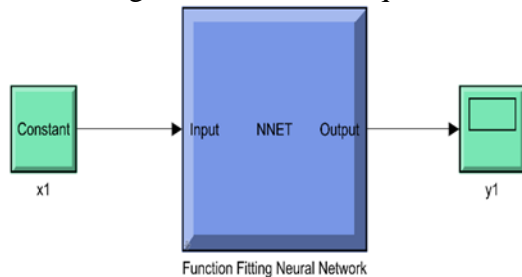


**Fig.14. Simulink developed by NN model**

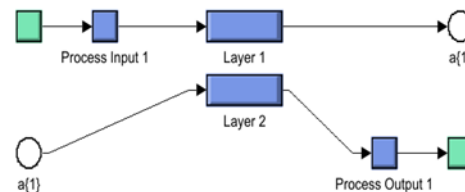


**Fig.15. Inner layers of Simulink developed**

The optimal ANN results were achieved, with variations within +/-1 volt.

## 3.2 INVERTER CONTROL FOR GRID INTEGRATION

A grid-connected inverted system's ability to manage the flow of Reactive and active power are dependent heavily on the d-q control. PCC voltage control is used to achieve d-q control. The d-axis control manages active power, adjusting it to match grid requirements or to maintain a stable DC-link voltage. Meanwhile, the q-axis control handles reactive power, ensuring a power factor close to unity. By independently controlling these parameters, the inverter optimizes energy transfer between renewable energy sources, grid. This control strategy allows for seamless integration of renewable energy, grid stability and reduced THD levels in output. The PI controller, employed in the d-axis control loop, fine tune the current reference to achieve precise power management, enhance the overall performance and reliability renewable energy grid integration. The voltage control is shown in fig 16.

Making use of the three different phase reference voltages  $U_a, U_b, U_c$ . we generate six PWM pulses that are utilized to drive this three-phase multilevel inverter [16].

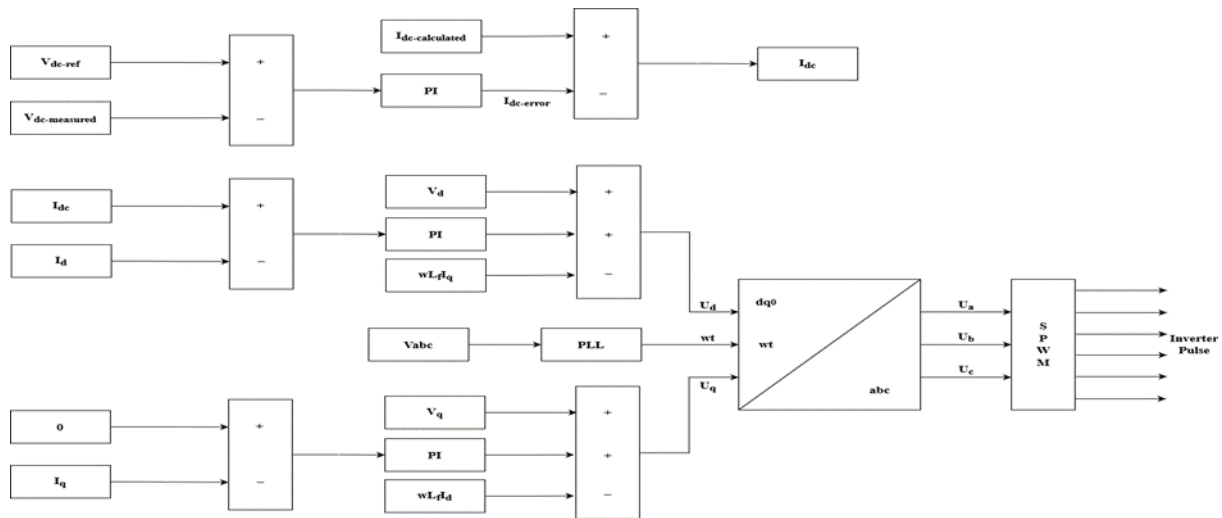


**Fig.16. DQ Voltage Control loop**

#### IV. RESULT

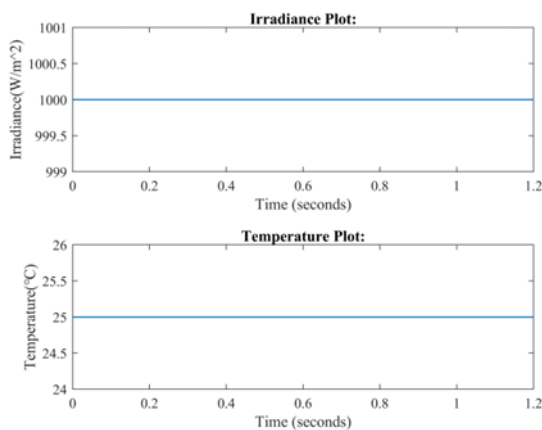
The Suggested ANN-based MPPT system with a modified SEPIC converter performs better for grid-integrated PV systems, attaining over 99.5% efficiency and steady power extraction with less than 1% variance. With a quick 0.04 second settling time and a THD of less than 0.66%, the dq-controlled inverter guarantees smooth grid integration. Maximizing energy harvesting which leads to produce more energy per unit of installed capacity, reducing the Levelized Cost of Energy (LCOE) and upholding excellent power quality.

Output waveforms under different Environmental Conditions are given below. the conditions are:

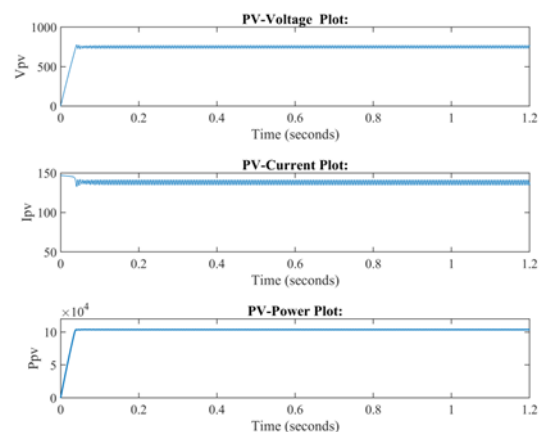
- A. With Constant Irradiance and Constant Temperature
- B. With Dynamic Irradiance and Constant Temperature
- C. With Constant Irradiance and Dynamic Temperature

##### A. with constant irradiance and constant temperature

Under these conditions, we are taking constant Irradiance of  $1000 \text{ W/m}^2$  and constant Temperature  $25 \text{ }^\circ\text{C}$  as discribed by Fig 17(a).

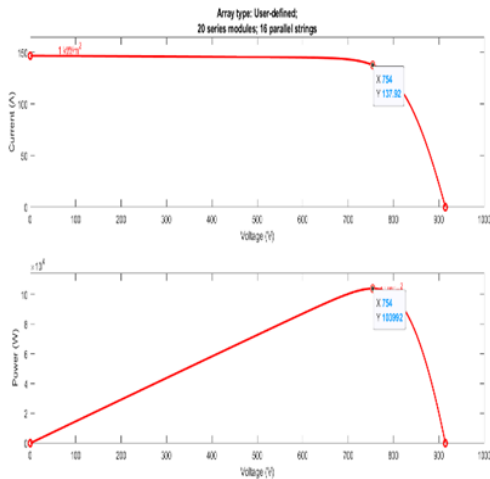


**Fig.17(a).Irradiance and Temperature**

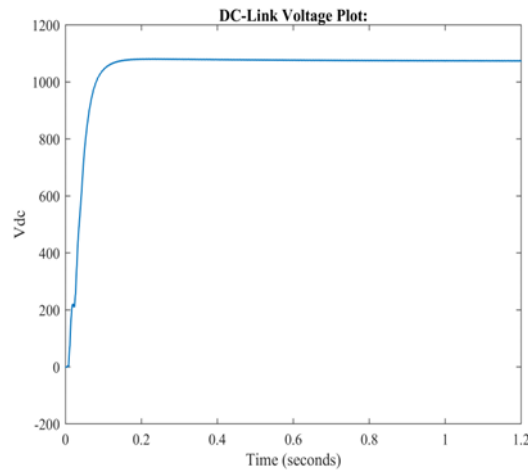


**Fig.17(b). Voltage,Current,Power polt of PV**

As demonstrated in Fig. 17(b), Voltage, Current, Power plot of PV were achieved at a constant temperature and irradiance of  $25\text{ }^{\circ}\text{C}$  and  $1000\text{ W/m}^2$ . Here, PV-Power fluctuate in between 103976.8 to 103072 watts, where its average is 103524.4 watts and the PV array's characteristic curve shows a maximum power point of 103992 watts as illustrated in fig 17(c). Therefore efficiency is 99.55% under these condition.



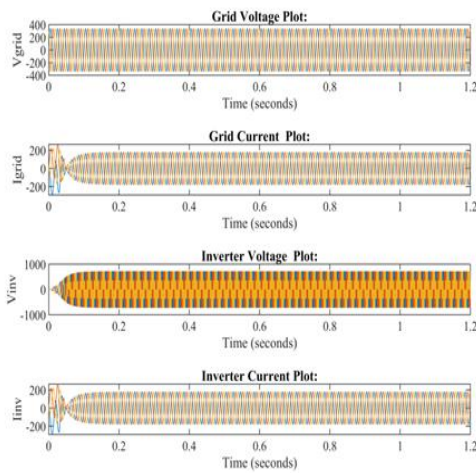
**Fig.17(c). PV array's characteristic curve**



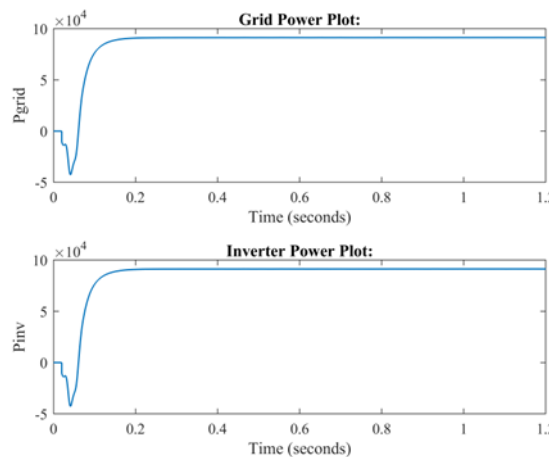
**Fig.17(d). DC-Link Voltage**

Fig 17(d) shows DC-Link Voltage which is maintained constant across the input of three phase inverter and Current and Voltage waveform across the inverter and grid are presented in Fig. 17(e) and THD for Inverter Current under these condition is given in table 3.

The Fig. 17(f) shows Power that obtained across the Inverter and Power integrated into grid.



**Fig.17(e). Grid & Inverter (Voltage & Current)**



**Fig.17(f). Grid Power & Inverter Power**

**B. With Dynamic Irradiance and Constant Temperature**

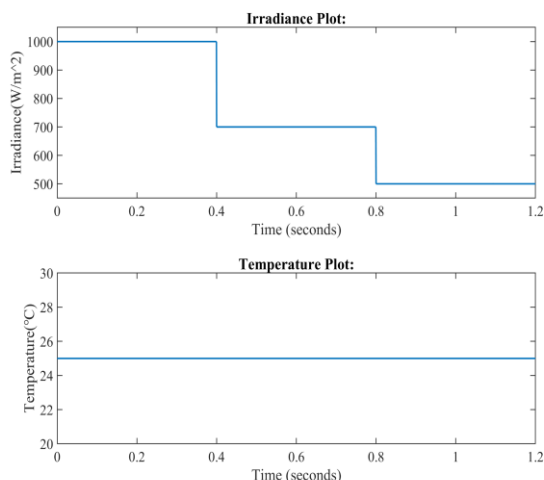


**Fig.18(a).Irradiance and Temperature**

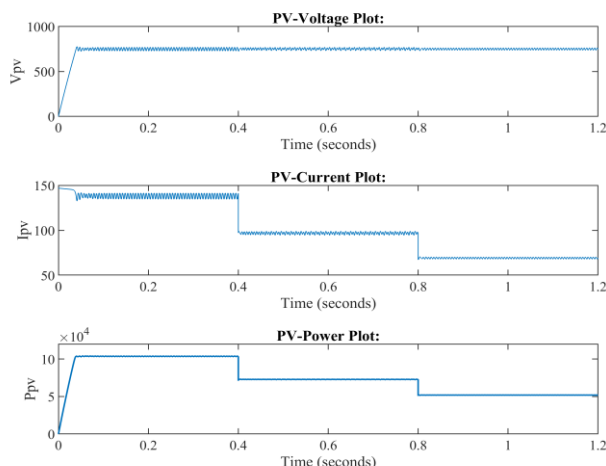


**Fig.18(b).Voltage,Current,Power plot of PV**

Under these conditions, we are taking dynamic Irradiance of ( $1000 \text{ W/m}^2$ ,  $700 \text{ W/m}^2$ ,  $500 \text{ W/m}^2$ ) and constant Temperature  $25^\circ\text{C}$  as described by Fig 18(a). Voltage, Current, Power plot of PV obtained under dynamic Irradiance of ( $1000 \text{ W/m}^2$ ,  $700 \text{ W/m}^2$ ,  $500 \text{ W/m}^2$ ) and constant Temperature  $25^\circ\text{C}$  as shown in Fig 18(b).

At  $1000 \text{ W/m}^2$  Irradiance PV-Power fluctuate in between 103982.2 to 103024.7 watts, where its average is 103503.45 watts and PV array's characteristic curve shows a maximum power point of 103992 watts as illustrated in fig 18(c). Therefore efficiency is 99.53% under these condition.

At  $700 \text{ W/m}^2$  Irradiance PV-Power fluctuate in between 72965.15 to 72417.68 watts, where its average is 72691.415 watts and PV array's characteristic curve shows a maximum power point of 72967 watts as illustrated in fig 18(c). Therefore efficiency is 99.62% under these condition.

At  $500 \text{ W/m}^2$  Irradiance PV-Power fluctuate in between 51960.34 to 51776.3 watts, where its average is 51868.15 watts and PV array's characteristic curve shows a maximum power point of 51868.15 watts as illustrated in fig 18(c). Therefore efficiency is 99.82% under these condition.

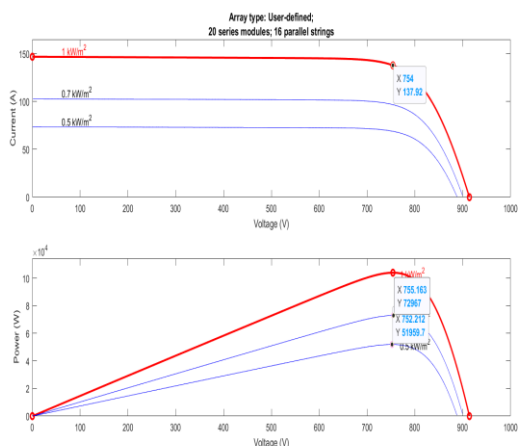


**Fig.18(c).PV array's characteristic curve**

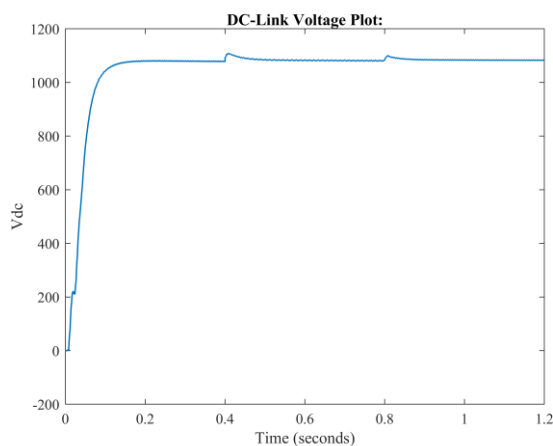


**Fig.18(d).DC-Link Voltage**

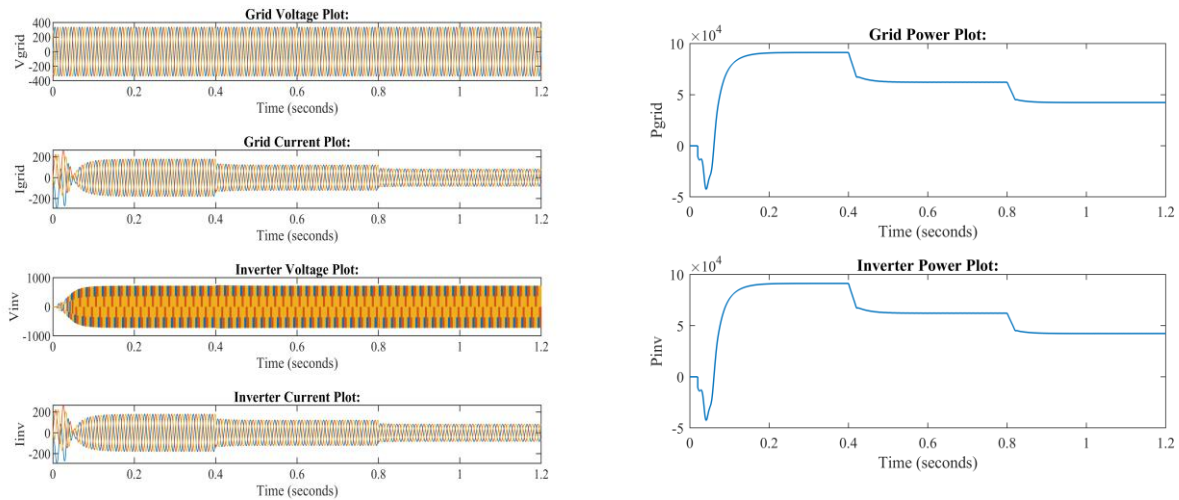


**Fig.18(e).Grid & Inverter (Voltage & Current)      Fig.18(f).Grid Power & Inverter Power**

Fig. 18(d) shows DC-Link Voltage which is maintained constant across the input of three phase inverter and Current and Voltage across the inverter and grid are presented in Fig 18(e) and THD for Inverter Current under these condition is given in table 3.

The Fig 18(f) shows Power that obtained across the Inverter and Power integrated into grid.

**C. With Constant Irradiance and Dynamic Temperature**

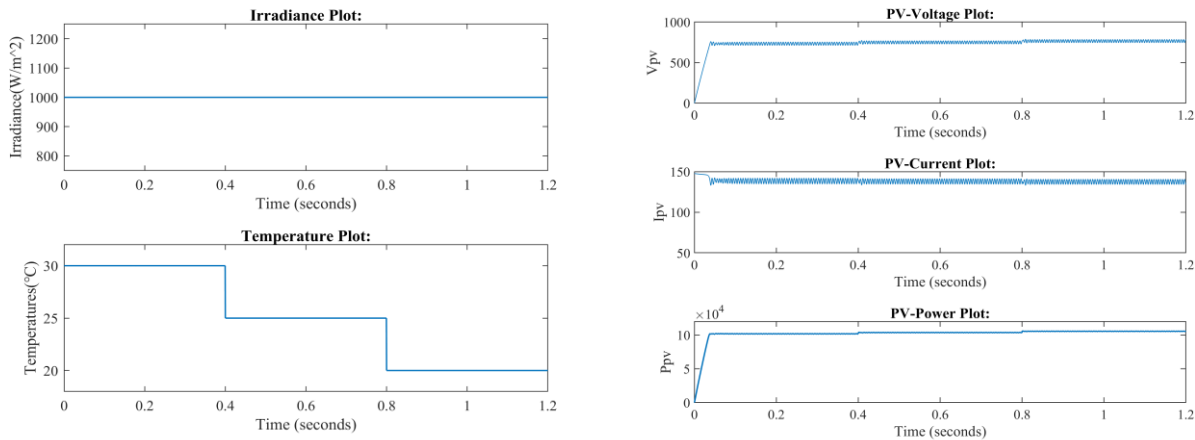


**Fig.19(a).Irradiance and Temperature      Fig.19(b).Voltage,Current,Power plot of PV**

Under these conditions, we are taking constant Irradiance of  $1000 \text{ W/m}^2$  and dynamic Temperature ( $30 \text{ }^\circ\text{C}$ ,  $25 \text{ }^\circ\text{C}$ ,  $20 \text{ }^\circ\text{C}$ ) as described by Fig 19(a). Voltage, Current, Power plot of PV obtained under constant Irradiance of  $1000 \text{ W/m}^2$  and dynamic Temperature of ( $30 \text{ }^\circ\text{C}$ ,  $25 \text{ }^\circ\text{C}$ ,  $20 \text{ }^\circ\text{C}$ ) as shown in Fig 19(b).

At  $30 \text{ }^\circ\text{C}$  Temperature PV-Power fluctuate in between 102134.1 to 101173.6 watts, where its average is 101653.85 watts and the PV array's characteristic curve shows a maximum power point of 102131 watts as illustrated in fig 19(c). Therefore efficiency is 99.53% under these condition.

At  $25 \text{ }^\circ\text{C}$  Temperature PV-Power fluctuate in between 103982.2 to 103075.9625 watts, where its average is 103529.0813 watts and the PV array's characteristic curve shows a maximum power point of 103992 watts as illustrated in fig 19(c). Therefore efficiency is 99.55% under these condition.

At  $20 \text{ }^\circ\text{C}$  Temperature PV-Power fluctuate in between 105808.8 to 104921.64 watts, where its average is 105365.22 watts and the PV array's characteristic curve shows a maximum power point of 105806 watts as illustrated in fig 19(c). Therefore efficiency is 99.58% under these condition.

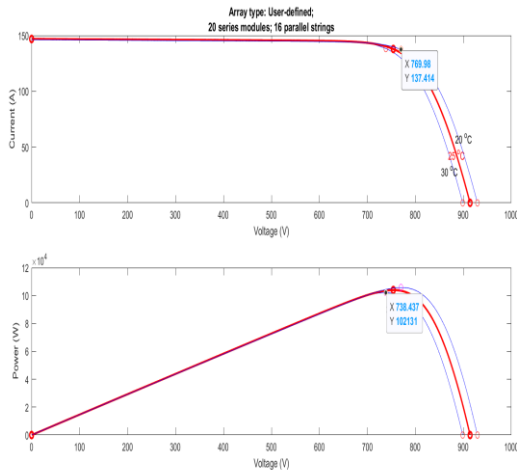


Fig.19(c).PV array's characteristic curve

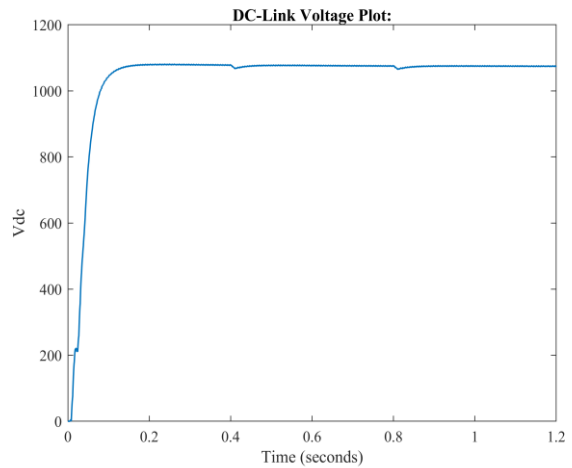


Fig.19(d) DC-Link Voltage

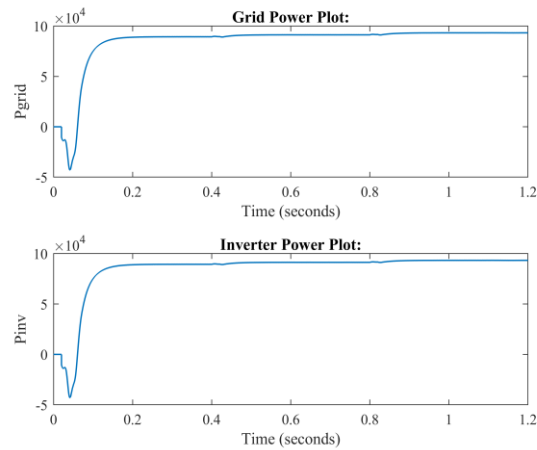
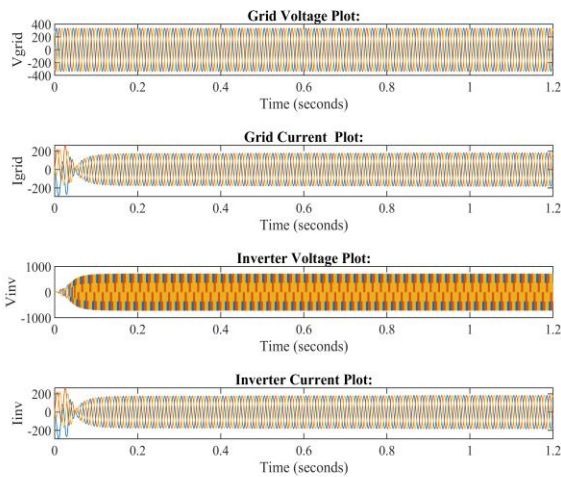


Fig.19(e).Grid & Inverter (Voltage & Current) Fig.19(f).Grid Power & Inverter Power

Fig 19(d) shows DC-Link Voltage which is maintained constant across the input of three phase inverter and Current and Voltage across the inverter and grid are presented in Fig 19(e) and THD for Inverter Current under these condition is given in table 3.

The Fig 19(f) shows Power that obtained across the Inverter and Power integrated into grid.

**Efficiency:**

**Table.II. Efficiency under different conditions**

| Environm ent Condition              | Irradiance ( $W/m^2$ ) | Temper a- ture ( $^{\circ}C$ ) | SIMULINK SCOPE RESULTS |                   |                   | PV- CURVE $P_{max-curve}$ (watts) | Efficiency $\frac{P_{avg}}{P_{max-curve}} * 100$ |
|-------------------------------------|------------------------|--------------------------------|------------------------|-------------------|-------------------|-----------------------------------|--|
|                                     |                        |                                | $P_{max}$ (watts)      | $P_{min}$ (watts) | $P_{avg}$ (watts) |                                   |  |
| Constant Irradiance and Temperature | 1000                   | 25                             | 103976.8               | 103072            | 103524.4          | 103992                            | 99.55%   |
| Dynamic Irradiance and Constant     | 1000                   | 25                             | 103982.2               | 103024.7          | 103503.45         | 103992                            | 99.53%   |
|                                     | 700                    | 25                             | 72965.15               | 72417.68          | 72691.415         | 72967                             | 99.62%   |

|   |      |    |          |            |            |          |        |
|---|------|----|----------|------------|------------|----------|--------|
| Temperature                                 | 500  | 25 | 51960.34 | 51776.3    | 51866.15   | 51868.15 | 99.82% |
| Constant Irradiance and Dynamic Temperature | 1000 | 30 | 102134.1 | 101173.6   | 101653.85  | 102131   | 99.53% |
|   | 1000 | 25 | 103982.2 | 103075.962 | 103529.081 | 103992   | 99.55% |
|   | 1000 | 20 | 105808.8 | 104921.64  | 105365.22  | 105806   | 99.58% |

Table II shows the extraction efficiency of system suggested under different conditions.

**Total harmonic disorder:**

**Table.III. THD under different conditions.**

| Environmental Condition                    | Irradiance (W/m <sup>2</sup> ) | Temperature (°C) | THD measured at (sec) | THD of Inverter Current |
|--|--------------------------------|------------------|-----------------------|-------------------------|
| Constant Irradiance & Constant Temperature | 1000                           | 25               | 0.8                   | 0.36%                   |
| Dynamic Irradiance & Constant Temperature  | 1000                           | 25               | 0.3                   | 0.40%                   |
|  | 700                            | 25               | 0.6                   | 0.55%                   |
|  | 500                            | 25               | 1                     | 0.66%                   |
| Constant Irradiance & Dynamic Temperature  | 1000                           | 30               | 0.3                   | 0.39%                   |
|  | 1000                           | 25               | 0.6                   | 0.37%                   |
|  | 1000                           | 20               | 1                     | 0.37%                   |

Table III shows the THD of inverter current during different Environmental Condition.

**V. CONCLUSION**

In summary, this study demonstrates that energy harvesting for Solar PV using a Modified SEPIC converter may be significantly enhanced by an ANN-based method. The ANN precisely estimated the Voltage at the Maximum Power Point by using temperature and solar irradiation as inputs and these MPPT methods can provide better efficiency, faster response, reduced hardware requirements, and improved performance under challenging conditions, all of which contribute to their cost-effectiveness and economical compared to traditional MPPT techniques . By the three-phase voltage management strategies, then has successfully stabilized the inverter output voltages and optimized grid tied power injection with reduction of harmonic distortion and also improve voltage quality.

**REFERENCES**

[1] P. K. Maroti, S. Padmanaban, J. B. Holm-Nielsen, M. Sagar Bhaskar, M. Meraj and A. Iqbal, "A New Structure of High Voltage Gain SEPIC Converter for Renewable Energy Applications," in IEEE Access, vol. 7, pp. 89857-89868, 2019, doi: 10.1109/ACCESS.2019.2925564.

[2]A. M. Mufsin, M. Shahin, C. M. Nirmal Mukundan and P. Jayaprakash, "A Modified SEPIC Converter Based Solar Power Integration with Single Phase Utility Bus," 2020 IEEE International Power and Renewable Energy Conference, Karunagappally,India,2020,pp.16,doi:10.1109/IPRECON49514.2020.9315251.

[3]N. Femia, G. Petrone, G. Spagnuolo and M. Vitelli, "Optimization of perturb and observe maximum power point tracking method," in IEEE Transactions on Power Electronics, vol. 20, no. 4, pp. 963973, July 2005, doi: 10.1109/TPEL.2005.850975.



- [4]A. Safari and S. Mekhilef, "Simulation and Hardware Implementation of Incremental Conductance MPPT With Direct Control Method Using Cuk Converter," in *IEEE Transactions on Industrial Electronics*, vol. 58, no. 4, pp. 1154-1161, April 2011, doi: 10.1109/TIE.2010.2048834.
- [5]L. Bouselham, B. Hajji and H. Hajji, "Comparative study of different MPPT methods for photovoltaic system," 2015 3rd International Renewable and Sustainable Energy Conference (IRSEC), Marrakech, Morocco, 2015, pp. 1-5, doi: 10.1109/IRSEC.2015.7455085.
- [6]Mani, D.R., Muthu, S. & Kasilingam, K. Enhanced power quality and efficient photovoltaic integration with a PV-based unified power quality conditioner using optimized MPPT technique. *Electr Eng* (2024). <https://doi.org/10.1007/s00202-024-02627-x>
- [7]Mishra, M., Mahajan, P. & Garg, R. Implementation and comparison of metaheuristically modified ANN MPPT controllers under varying solar irradiance conditions. *Electr Eng* **106**, 3427–3443 (2024). <https://doi.org/10.1007/s00202-023-02165-y>
- [8]R. W. Erickson and D. Maksimovic, *Fundamentals of Power Electronics*, 2nd ed. Norwell, MA, USA: Kluwer, 2001.
- [9]Y. Tang, T. Wang and Y. He, "A Switched-Capacitor-Based Active-Network Converter With High Voltage Gain," in *IEEE Transactions on Power Electronics*, vol.29,no.6,pp.29592968,June2014,doi:10.1109/TPEL.2013.2272639.
- [10] R. Gules, W. M. dos Santos, F. A. dos Reis, E. F. R. Romaneli and A. A. Badin, "A Modified SEPIC Converter With High Static Gain for Renewable Applications," in *IEEE Transactions on Power Electronics*, vol. 29, no. 11, pp. 5860-5871, Nov. 2014, doi: 10.1109/TPEL.2013.2296053.
- [11] A. R. Suryawanshi and N. B. Chopade, "Multilevel Inverter Topologies and Modulation Techniques for Grid Connection of Renewable Energy Source," 2019 International Conference on Innovative Trends and Advances in Engineering and Technology (ICITAET), Shegoan, India, 2019, pp. 227232, doi: 10.1109/ICITAET47105.2019.9170239.
- [12] S. Nayak, S. Gurunath and N. Rajasekar, "Advanced single-phase inverse park PLL with tuning of PI controller for improving stability of grid utility using soft computing technique," 2016 Online International Conference on Green Engineering and Technologies (IC-GET), Coimbatore, India, 2016, pp. 1-5, doi: 10.1109/GET.2016.7916732.
- [13] Karthik, M., Naik, N.V.R. & Panda, A.K. A robust generalized soft-root-sign adaptive filter algorithm for a grid-coupled PV system. *Electr Eng* **106**, 2537–2553 (2024). <https://doi.org/10.1007/s00202-023-02097-7>
- [14] F. Shaikh and B. Joseph, "Simulation of synchronous reference frame PLL for grid synchronization using Simulink," 2017 International Conference on Advances in Computing, Communication and Control (ICAC3), Mumbai, India, 2017, pp. 1-6, doi: 10.1109/ICAC3.2017.8318790.
- [15] "Power Inverter," Sep.24, 2019. Accessed on: Oct. 3, 2019. [Online]. Available: [https://en.wikipedia.org/wiki/Power\\_inverter](https://en.wikipedia.org/wiki/Power_inverter)
- [16] Mr. M.Nagaiyah, Mr. J.Chaitanya Krishna, Dr. Shaik Rafi Kiran," Application of Multilevel Inverters in Solar, Battery and Wind hybrid System for Domestic Load Application" *International Journal of Advanced Engineering Research and Science (IJAERS) Trends in Engineering and Technology (NCTET-2K17)*,DOI: [10.22161/ijaers/nctet.2017.eee.1](https://doi.org/10.22161/ijaers/nctet.2017.eee.1)
- [17] M. Suthar, G. K. Singh and R. P. Saini, "Comparison of mathematical models of photo-voltaic (PV) module and effect of various parameters on its performance," 2013 International Conference on Energy Efficient Technologies for Sustainability, Nagercoil, India, 2013, pp. 1354-1359, doi: 10.1109/ICEETS.2013.6533584.
- [18] M.A. Hasan, S.K. Parida," Alytical And Explan Over View Of Solar Photovoltaic Panel Modeling Based On Anerimental View Point",*Renewable and Sustainable Energy Reviews*,vol. 60, pp. 75-83,Jul.2016.



- [19] M. G. Villalva, J. R. Gazoli and E. R. Filho, "Comprehensive Approach to Modeling and Simulation of Photovoltaic Arrays," in *IEEE Transactions on Power Electronics*, vol. 24, no. 5, pp. 1198-1208, May 2009, doi: [10.1109/TPEL.2009.2013862](https://doi.org/10.1109/TPEL.2009.2013862).
- [20] S. B. Dewan and P. D. Ziogas, "Optimum filter design for a single-phase solid-state UPS system," *IEEE Trans. Ind Appl.*, vol. IA-15, no. 6, pp. 664–669, Nov. 1979.
- [21] S. Jayalath and M. Hanif, "Generalized LCL-filter design algorithm for grid-connected voltage-source inverter," *IEEE Trans. Ind. Electron.*, vol. 64, no. 3, pp. 1905–1915, Mar. 2017.
- [22] D. Dong et al., "A PV residential microinverter with grid-support function: Design, implementation, and field testing," *IEEE Trans. Ind Appl.*, vol. 54, no. 1, pp. 469–481, Jan./Feb. 2018.
- [23] Z. Zou, Z. Wang, and M. Cheng, "Modeling, analysis, and design of multifunction grid-interfaced inverters with output LCL filter," *IEEE Trans. Power Electron.*, vol. 29, no. 7, pp. 3830–3839, Jul. 2014.
- [24] Bendib, B.; Krim, F.; Belmili, H.; Almi, M.F.; Bolouma, S., "An intelligent MPPT approach based on neural-network voltage estimator and fuzzy controller, applied to a stand-alone PV system," *Industrial Electronics (ISIE)*, proceedings of IEEE 23rd International Symposium on , vol.no., pp.404,409, 1-4 June 2014.
- [25] W. Lee, K. Kim, J. Park, J. Kim, and Y. Kim, "Forecasting solar power using long-short term memory and convolutional neural networks," *IEEE Access*, vol. 6, pp. 73068–73080, 2018, doi: [10.1109/ACCESS.2018.2883330](https://doi.org/10.1109/ACCESS.2018.2883330).
- [26] S. Al-Dahidi, O. Ayadi, M. Alrbai, and J. Adeeb, "Ensemble approach of optimized artificial neural networks for solar photovoltaic power prediction," *IEEE Access*, vol. 7, pp. 81741–81758, 2019, doi: [10.1109/ACCESS.2019.2923905](https://doi.org/10.1109/ACCESS.2019.2923905).
- [27] M. Sinecen, "Comparison of genomic best linear unbiased prediction and Bayesian regularization neural networks for genomic selection," *IEEE Access*, vol. 7, pp. 79199–79210, 2019, doi: [10.1109/ACCESS.2019.2922006](https://doi.org/10.1109/ACCESS.2019.2922006).